

NASA Contractor Report 3483

NASA-CR-3483

19820004972

HAMPTON, VIRGINIA

Deep Anisotropic Shell Program for Tire Analysis

FOR REFERENCE

NOT TO BE TAKEN FROM THIS ROOM

Carl M. Andersen

CONTRACT NAS1-15965
NOVEMBER 1981

NASA



NF02154

NASA Contractor Report 3483

Deep Anisotropic Shell Program for Tire Analysis

Carl M. Andersen
The College of William and Mary
Williamsburg, Virginia

Prepared for
Langley Research Center
under Contract NAS1-15965



National Aeronautics
and Space Administration

**Scientific and Technical
Information Branch**

1981

SUMMARY

A finite element program has been constructed to model the mechanical response of a tire, treated as a deep anisotropic shell, to specified static loads. The program is based on a Sanders-Budiansky type shell theory with the effects of transverse shear deformation and bending-extensional coupling included. A displacement formulation is used together with a total Lagrangian description of the deformation. Sixteen-node quadrilateral elements with bicubic shape functions are employed. The Noor basis reduction technique and various types of symmetry considerations serve to improve the computational efficiency.

INTRODUCTION

The study of the behavior of aircraft tires by analytical methods presents many challenges. Any significant tire computations must involve the solution of systems of equations which are highly nonlinear and should account for a variety of physical effects, such as anisotropic and nonhomogeneous material properties, large deformations, the generation of heat, and the interaction between thermal and material characteristics. Thus a considerable amount of mathematical and programming effort is needed to keep the computation costs within reason.

The purpose of this report is to describe a finite element computer program designed as a first step in a tire analysis project. The program is limited to a nonlinear analysis of a laminated anisotropic linearly elastic shell subjected to static conservative loading. A Sanders-Budiansky type deep-shell theory (refs. 1 and 2) is employed with the effects of transverse shear deformation and bending-extensional coupling included. Normals to the undeformed shell reference surface are assumed to remain straight lines in the deformed shell, and rotations are assumed to be moderate but not large. The undeformed shell is assumed to be axisymmetric and to have elliptic cross section; although other more general cross sections can be easily accommodated. The program is based on a total-Lagrangian displacement formulation with five fundamental unknowns. Sixteen-node bicubic quadrilateral elements are employed; and, thus, there are 80 degrees of freedom associated with each finite element. The necessary integrals are evaluated through the use of numerical quadrature.

The coordinate directions are chosen to be along the principal lines of curvature, and the elements are rectangular with respect to the surface coordinates. Due to the large sizes of the arrays of stiffness coefficients generated, a computational strategy is employed which requires that only portions of the arrays be in central memory at any given time. Permutational symmetry is exploited to reduce the amount of storage used. The Noor basis reduction technique [refs. 3 through 6] is used in the program to reduce the computational expense.

Two sample problems are solved using the computer program. Both involve toroidal shells with static uniform pressure loading, and the solutions exhibit axial and reflection symmetries.

SYMBOLS

A_{α}	coefficients of first fundamental form
a	semimajor axis of cross section
a_{α}	curvature quantities defined in equation (7)
$a_{\alpha,i}$	strain approximation functions defined in equation (20)
$a_{\alpha,i,q}$	values of strain approximation functions at quadrature points
B_{11}, B_{22}	components of second fundamental form
b	toroidal radius
$C_{\alpha\beta} (\alpha, \beta = 1, 2, 6)$	extensional stiffnesses of shell
$C_{\alpha\beta} (\alpha, \beta = 4, 5)$	shear stiffnesses of shell
$\bar{C}_{\lambda\mu}$	composite matrix of shell stiffnesses
c	distance between beads of tire
$D_{\alpha\beta} (\alpha, \beta = 1, 2, 6)$	bending stiffnesses
\mathcal{D}_{α}	differential operators defined in equation (8)
$\mathcal{D}_{\alpha}^{(+)}$	differential operators defined in equation (8)
$\mathcal{D}_{\alpha}^{(-)}$	differential operators defined in equation (8)
$D_{\alpha,i}$	strain approximation functions defined in equation (20)
$D_{\alpha,i}^{(+)}$	strain approximation functions defined in equation (20)
$D_{\alpha,i}^{(-)}$	strain approximation functions defined in equation (20)
$D_{\alpha,i,q}$	values of strain approximation functions defined in equation (20)
$D_{\alpha,i,q}^{(+)}$	values of strain approximation functions defined in equation (20)
$D_{\alpha,i,q}^{(-)}$	values of strain approximation functions defined in equation (20)
E	Young's modulus of isotropic material
E_L, E_T	Elastic moduli parallel to and perpendicular to the tire cords, respectively

$F_{\alpha\beta}$ ($\alpha, \beta = 1, 2, 6$)	stiffness interaction coefficients of shell
F_{ijk}^{IJK}	array of nonlinear stiffness coefficients
G_{ijkl}^{IJKL}	array of nonlinear stiffness coefficients
G_{LT}, G_{TT}	shear moduli in plane of cords and normal to it, respectively
h	thickness of shell
K_{α}	differential operator defined in equation (8)
$K_{\alpha,i}$	strain approximation functions defined in equation (20)
$K_{\alpha,i,q}$	values of strain approximation functions at quadrature points
K_{ij}^{IJ}	linear stiffness coefficients
k_1, k_2	curvatures of shell
$M_{\alpha\beta}$	bending stress resultants
$N_{\alpha\beta}$	extensional stress resultants
N_i	shape functions
n_q	number of quadrature points
p_{α}, p	external load intensities in coordinate directions
Q_{α}	transverse shear stress resultants
U	strain energy of shell
u_{α}, w	displacement components in coordinate directions
W	work done by external forces
X_{α}	lines of curvature surface coordinates
x_1, x_2, x_3	Cartesian coordinates
$\gamma_{\alpha,q}$	quantities defined in equation (25)
$\epsilon_{\alpha\beta}$	extensional strains
$\epsilon_{\alpha 3}$	transverse shear strains
$\epsilon_{\lambda,q}$	values of strains at quadrature points
$\kappa_{\alpha\beta}$	curvature changes and twist of shell reference surface

ν	Poisson's ratio for isotropic materials
ν_{LT}	Poisson's ratio measuring strain in transverse direction due to uniaxial normal stress in direction of cords
Π	Governing functional to be minimized
$\sigma_{\lambda,q}$	values of stress resultants at quadrature points
$\sigma_{\lambda,i,q}^I$	quantities related to linear part of stress, definition in equation (28)
ϕ_α	shell rotation components
ϕ	shell rotation about the normal to the surface
ϕ_q	values of normal rotation at quadrature points
ψ_i^I	nodal displacement parameters
Ω	shell domain

Unless otherwise specified the ranges of the indices are as follows:

$$\begin{aligned}
 \alpha, \beta &= 1, 2 \\
 \lambda, \mu &= 1 \rightarrow 8 \\
 i, j, k, l &= 1 \rightarrow 16 \\
 I, J, K, L &= 1 \rightarrow 5 \\
 q &= 1 \rightarrow n_q
 \end{aligned}$$

MATHEMATICAL FORMULATION

The mathematical formulation is based on a Sanders-Budiansky type deep shell theory which includes the effects of transverse shear deformation, anisotropic material behavior and bending-extensional coupling. A total Lagrangian description of the shell deformation is used and the shell configurations are referred to lines of curvature coordinates of the undeformed shell. Only static deformations are considered, and the initial configuration of the shell is assumed to be a momentless state. A displacement formulation is used in which the fundamental unknowns consist of five generalized displacements -- the two tangential displacement components, u_1 and u_2 ; the normal displacement w ; and the two rotation

components ϕ_1 and ϕ_2 . The generalized displacements are shown schematically in Figure 1. The shell stiffness coefficients are obtained by using the principle of minimum potential energy.

The Governing Functional

The governing functional employed in this study is given by

$$\Pi(u_1, u_2, w, \phi_1, \phi_2) = U - W \quad (1)$$

where U is the strain energy due to deformation and W is the potential energy of the external forces. The expression for W in terms of the displacements u_1, u_2 and w is

$$W = \int_{\Omega} (p_1 u_1 + p_2 u_2 + p w) d\Omega \quad (2)$$

where p_1, p_2 and p are given external load intensities (see Fig. 1) and Ω is the shell domain.

The strain energy is expressed in terms of the strains, $\epsilon_{11}, \epsilon_{22}, \epsilon_{12}, \kappa_{11}, \kappa_{22}, \kappa_{12}, \epsilon_{13}$ and ϵ_{23} , and the stress resultants $N_{11}, N_{22}, N_{12}, M_{11}, M_{22}, M_{12}, Q_1$ and Q_2 , by

$$U = \int_{\Omega} (\epsilon_{11} N_{11} + \epsilon_{22} N_{22} + 2 \epsilon_{12} N_{12} + \kappa_{11} M_{11} + \kappa_{22} M_{22} + 2 \kappa_{12} M_{12} + 2 \epsilon_{13} Q_1 + 2 \epsilon_{23} Q_2) d\Omega \quad (3)$$

The stress-strain relations are assumed to be linear and to have the form

$$\begin{bmatrix} N_{11} \\ N_{22} \\ N_{12} \\ M_{11} \\ M_{22} \\ M_{12} \\ Q_1 \\ Q_2 \end{bmatrix} = \begin{bmatrix} C_{11} & C_{12} & C_{16} & F_{11} & F_{12} & F_{16} & 0 & 0 \\ C_{12} & C_{22} & C_{26} & F_{12} & F_{22} & F_{26} & 0 & 0 \\ C_{16} & C_{26} & C_{66} & F_{16} & F_{26} & C_{66} & 0 & 0 \\ F_{11} & F_{12} & F_{16} & D_{11} & D_{12} & D_{16} & 0 & 0 \\ F_{12} & F_{22} & F_{26} & D_{12} & D_{22} & D_{26} & 0 & 0 \\ F_{16} & F_{26} & F_{66} & D_{16} & D_{26} & D_{66} & 0 & 0 \\ 0 & 0 & 0 & 0 & 0 & 0 & C_{55} & C_{54} \\ 0 & 0 & 0 & 0 & 0 & 0 & C_{54} & C_{44} \end{bmatrix} \begin{bmatrix} \epsilon_{11} \\ \epsilon_{22} \\ 2 \epsilon_{12} \\ \kappa_{11} \\ \kappa_{22} \\ 2 \kappa_{12} \\ 2 \epsilon_{13} \\ 2 \epsilon_{23} \end{bmatrix} \quad (4)$$

where the C's, D's and F's are the extensional, bending and stiffness interaction coefficients, respectively, appropriate for a laminated anisotropic shell.

For a shell in which the directions of principal curvature, k_1 and k_2 , are along the coordinate directions the strain-displacement relations may be represented by

$$\begin{pmatrix} \epsilon_{11} \\ \epsilon_{22} \\ 2 \epsilon_{12} \\ \kappa_{11} \\ \kappa_{22} \\ 2 \kappa_{12} \\ 2 \epsilon_{13} \\ 2 \epsilon_{23} \end{pmatrix} = \begin{pmatrix} \mathcal{D}_1 & a_2 & k_1 & 0 & 0 \\ a_1 & \mathcal{D}_2 & k_2 & 0 & 0 \\ \mathcal{D}_2^{(-)} & \mathcal{D}_1^{(-)} & 0 & 0 & 0 \\ 0 & 0 & 0 & \mathcal{D}_1 & a_2 \\ 0 & 0 & 0 & a_1 & \mathcal{D}_2 \\ K_2 & K_1 & 0 & \mathcal{D}_2^{(-)} & \mathcal{D}_1^{(-)} \\ -k_1 & 0 & \mathcal{D}_1 & 1 & 0 \\ 0 & -k_2 & \mathcal{D}_2 & 0 & 1 \end{pmatrix} \begin{pmatrix} u_1 \\ u_2 \\ w \\ \phi_1 \\ \phi_2 \end{pmatrix} + \begin{pmatrix} (1/2)(k_1 u_1 - \mathcal{D}_1 w)^2 + (1/2)\phi^2 \\ (1/2)(k_2 u_2 - \mathcal{D}_2 w)^2 + (1/2)\phi^2 \\ (k_1 u_1 - \mathcal{D}_1 w)(k_2 u_2 - \mathcal{D}_2 w) \\ 0 \\ 0 \\ 0 \\ 0 \\ 0 \end{pmatrix} \quad (5)$$

where ϕ , the rotation about the normal to the shell, is given by

$$\phi = (1/2) (\mathcal{D}_1^{(+)} u_2 - \mathcal{D}_2^{(+)} u_1) \quad (6)$$

the quantities a_1 and a_2 are given by

$$a_\alpha = (A_1 \ A_2)^{-1} \partial A_{3-\alpha} / \partial X_\alpha \quad (\alpha = 1, 2; \text{ no sum}) \quad (7)$$

and A_1 and A_2 are quantities related to the first fundamental form of the shell reference surface (see below). In equations (5) and (6) \mathcal{D}_α , $\mathcal{D}_\alpha^{(+)}$, $\mathcal{D}_\alpha^{(-)}$ and K_α are differential operators defined by

$$\begin{aligned} \mathcal{D}_\alpha f &= (A_\alpha)^{-1} \partial f / \partial X_\alpha \\ \mathcal{D}_\alpha^{(+)} f &= \mathcal{D}_\alpha f + a_\alpha f \\ \mathcal{D}_\alpha^{(-)} f &= \mathcal{D}_\alpha f - a_\alpha f \\ K_\alpha f &= (1/2) (k_{3-\alpha} - k_\alpha) \mathcal{D}_\alpha^{(+)} f \end{aligned} \quad (\alpha = 1, 2; \text{ no sum}) \quad (8)$$

where f is any function defined on the shell domain. Through the use of equations (1) to (8) the functional Π can be expressed as a function of the five generalized displacements, the stiffness of the material, and the geometry of the shell surface.

Surface Coordinates and Geometry

The reference surface of the undeformed tire is approximated by a toroid with surface coordinates X_1 and X_2 ; and the coordinate directions are chosen to be along the lines of principal curvature. The first and second fundamental forms of the surface then are

$$(A_1)^2 dX_1^2 + (A_2)^2 dX_2^2 \quad (9)$$

and

$$B_{11} dX_1^2 + B_{22} dX_2^2, \quad (10)$$

respectively. The curvatures of the shell surface along the coordinate directions are thus

$$\begin{aligned} k_1 &= -B_{11}/(A_1)^2 \\ k_2 &= -B_{22}/(A_2)^2 \end{aligned} \quad (11)$$

and the twist k_{12} is zero.

For such a surface the surface integrals appearing in equations (2) and (3) may be written as

$$\int_{\Omega} \dots d\Omega = \int_0^{2\pi} A_1 \int_0^{2\pi} A_2 \dots dX_2 dX_1 \quad (12)$$

Mathematically the simplest choice of toroid is the torus, a toroid with circular cross section. Let the cross-sectional radius be a and the toroidal radius be b . In this case the Cartesian coordinates are

$$\begin{aligned} x_1 &= (b + a \sin X_1) \sin X_2 \\ x_2 &= a \cos X_1 \\ x_3 &= (b + a \sin X_1) \cos X_2 \end{aligned} \quad (13)$$

and

$$\begin{aligned}
A_1 &= a \\
A_2 &= b + a \sin X_1 \\
B_{11} &= -a \\
B_{22} &= -(b + a \sin X_1) \sin X_1
\end{aligned}
\tag{14}$$

Consequently,

$$\begin{aligned}
k_1 &= a^{-1} \\
k_2 &= (b + a \sin X_1)^{-1} \sin X_1
\end{aligned}
\tag{15}$$

A surface which is nearly as simple to represent mathematically but somewhat more appropriate for representing an aircraft tire is a toroid whose cross section is an ellipse with eccentricity e , semimajor axis a , and semiminor axis $a\sqrt{1 - e^2}$. In this case

$$\begin{aligned}
x_1 &= \left[b + \frac{a (1 - e^2) \sin X_1}{1 + e \cos X_1} \right] \sin X_2 \\
x_2 &= -\frac{a (e + \cos X_1)}{1 + e \cos X_1} \\
x_3 &= \left[b + \frac{a (1 - e^2) \sin X_1}{1 + e \cos X_1} \right] \cos X_2
\end{aligned}
\tag{16}$$

and

$$\begin{aligned}
A_1 &= a (1 - e^2) (1 + e \cos X_1)^{-2} [1 + e (2 \cos X_1 + e)]^{1/2} \\
A_2 &= b + a (1 - e^2) \sin X_1 (1 + e \cos X_1)^{-1} \\
B_{11} &= -a (1 - e^2) (1 + e \cos X_1)^{-1} [1 + e (2 \cos X_1 + e)]^{-1/2} \\
B_{22} &= -A_2 \sin X_1 [1 + e (2 \cos X_1 + e)]^{-1/2} \\
k_1 &= [a (1 - e^2)]^{-1} (1 + e \cos X_1)^3 [1 + e (2 \cos X_1 + e)]^{-3/2} \\
k_2 &= A_2^{-1} \sin X_1 [1 + e (2 \cos X_1 + e)]^{-1/2}
\end{aligned}
\tag{17}$$

More accurate representations of the cross section of a particular tire geometry may be gained by the use of such forms as

$$\begin{aligned} x_1 &= [b + f(X_1)] \sin X_2 \\ x_2 &= g(X_1) \\ x_3 &= [b + f(X_1)] \cos X_2 \end{aligned} \quad (18)$$

where f and g are suitably chosen functions. The use of these more elaborate cross sections would require little additional computational effort.

Finite Element Discretization

Each of the five generalized displacements are approximated within a given finite element domain with the use of the same set of bicubic shape functions. Thus within an element

$$\begin{aligned} u_1 &= \psi_i^1 N_i \\ u_2 &= \psi_i^2 N_i \\ w &= \psi_i^3 N_i \\ \phi_1 &= \psi_i^4 N_i \\ \phi_2 &= \psi_i^5 N_i \end{aligned} \quad (i = 1 \rightarrow 16) \quad (19)$$

where $N_i = N_i(X_1, X_2)$ and repeated indices imply summation. The lower case Latin indices range from 1 to 16.

Since the differential operators of equations (5), (6) and (8), in effect, act only on the shape functions N_i , a set of "strain approximation functions" is introduced

$$\begin{aligned} D_{\alpha,i}(X_1, X_2) &= \mathcal{D}_{\alpha} N_i(X_1, X_2) \\ D_{\alpha,i}^{(+)}(X_1, X_2) &= \mathcal{D}_{\alpha}^{(+)} N_i(X_1, X_2) \\ D_{\alpha,i}^{(-)}(X_1, X_2) &= \mathcal{D}_{\alpha}^{(-)} N_i(X_1, X_2) \\ K_{\alpha,i}(X_1, X_2) &= K_{\alpha} N_i(X_1, X_2) \end{aligned} \quad (\alpha = 1, 2) \quad (20)$$

$$k_{\alpha,i}(X_1, X_2) = k_{\alpha} N_i(X_1, X_2)$$

$$a_{\alpha,i}(X_1, X_2) = a_{\alpha} N_i(X_1, X_2)$$

Further, since the integrals in equations (2) and (3) are to be evaluated through the use of numerical quadrature, only the values of the resulting functions at the quadrature points $(X_{1,q}, X_{2,q})$ are of interest. Accordingly, let

$$\begin{aligned} N_{i,q} &= N_i(X_{1,q}, X_{2,q}) \\ D_{\alpha,i,q} &= D_{\alpha,i}(X_{1,q}, X_{2,q}) \\ D_{\alpha,i,q}^{(+)} &= D_{\alpha,i}^{(+)}(X_{1,q}, X_{2,q}) \\ D_{\alpha,i,q}^{(-)} &= D_{\alpha,i}^{(-)}(X_{1,q}, X_{2,q}) \quad (\alpha = 1, 2; i = 1 \rightarrow 16; q = 1 \rightarrow n_q) \\ K_{\alpha,i,q} &= K_{\alpha,i}(X_{1,q}, X_{2,q}) \\ k_{\alpha,i,q} &= k_{\alpha,i}(X_{1,q}, X_{2,q}) \\ a_{\alpha,i,q} &= a_{\alpha,i}(X_{1,q}, X_{2,q}) \end{aligned} \quad (21)$$

where n_q is the number of quadrature points per element. Then the values of the strains at the quadrature points are

$$\varepsilon_{\lambda,q} = \varepsilon_{\lambda,q}^{(L)} + \varepsilon_{\lambda,q}^{(NL)} \quad (\lambda = 1 \rightarrow 8) \quad (22)$$

where the linear part of the strain is

$$\varepsilon_{\lambda,q}^{(L)} = \begin{pmatrix} D_{1,i,q} & a_{2,i,q} & k_{1,i,q} & 0 & 0 \\ a_{1,i,q} & D_{2,i,q} & k_{2,i,q} & 0 & 0 \\ D_{2,i,q}^{(-)} & D_{1,i,q}^{(-)} & 0 & 0 & 0 \\ 0 & 0 & 0 & D_{1,i,q} & a_{2,i,q} \\ 0 & 0 & 0 & a_{1,i,q} & D_{2,i,q} \\ K_{2,i,q} & K_{1,i,q} & 0 & D_{2,i,q}^{(-)} & D_{1,i,q}^{(-)} \\ -k_{1,i,q} & 0 & D_{1,i,q} & N_{1,q} & 0 \\ 0 & -k_{2,i,q} & D_{2,i,q} & 0 & N_{1,q} \end{pmatrix} \begin{pmatrix} \psi_i^1 \\ \psi_i^2 \\ \psi_i^3 \\ \psi_i^4 \\ \psi_i^5 \end{pmatrix} \quad (23)$$

and the nonlinear part is

$$\varepsilon_{\lambda,q}^{(NL)} = \begin{pmatrix} (1/2) \gamma_{1,q} \gamma_{1,q} + (1/2) \phi_q \phi_q \\ (1/2) \gamma_{2,q} \gamma_{2,q} + (1/2) \phi_q \phi_q \\ \phi_{1,q} \phi_{2,q} \\ 0 \\ 0 \\ 0 \\ 0 \\ 0 \end{pmatrix} \quad (24)$$

where

$$\begin{aligned} \gamma_{\alpha,q} &= k_{\alpha,i,q} \psi_{\alpha}^i - D_{\alpha,i,q} \psi_3^i \quad (\alpha = 1,2; \text{no sum on } \alpha) \\ \phi_q &= (1/2) (D_{1,i,q}^{(+)} \psi_2^i - D_{2,i,q}^{(+)} \psi_1^i) \end{aligned} \quad (25)$$

Equation (23) may be written more concisely in the form

$$\varepsilon_{\lambda,q}^{(L)} = \varepsilon_{\lambda,i,q}^I \psi_i^I \quad (\lambda = 1 \rightarrow 8; q = 1 \rightarrow n_q) \quad (26)$$

wherein I is summed from 1 to 5 and i is summed from 1 to 16.

The values of the stress resultants at the quadrature point q are given by

$$\sigma_{\lambda,q} = \sigma_{\lambda,q}^{(L)} + \sigma_{\lambda,q}^{(NL)} = \bar{C}_{\lambda\mu} (\varepsilon_{\mu,q}^{(L)} + \varepsilon_{\mu,q}^{(NL)}) \quad (\lambda = 1 \rightarrow 8; q = 1 \rightarrow n_q) \quad (27)$$

where $\bar{C}_{\lambda\mu}$ ($\lambda, \mu = 1 \rightarrow 8$) is the matrix appearing in equation (4). The use of numerical quadrature and the presence of Jacobians brings in a set of weights w_q ($q = 1 \rightarrow n_q$). It seems useful to define a set of quantities $\sigma_{\lambda,i,q}^I$ by

$$\begin{aligned} w_q \sigma_{\lambda,q}^{(L)} &= w_q \bar{C}_{\lambda\mu} \varepsilon_{\mu,q}^{(L)} = w_q \bar{C}_{\lambda\mu} \varepsilon_{\mu,i,q}^I \psi_i^I \\ &= \sigma_{\lambda,i,q}^I \psi_i^I \quad (\lambda = 1 \rightarrow 8; q = 1 \rightarrow n_q) \end{aligned} \quad (28)$$

where I is summed from 1 to 5 and i is summed from 1 to 16.

By using the above approximations to the governing functional Π in terms of the ψ_i^I , by summing over the quadrature points, and by differentiation with respect to ψ_i^I , the discretized equations for an element are seen to have the general form

$$K_{ij}^{IJ} \psi_j^J + (1/2) F_{ijk}^{IJK} \psi_j^J \psi_k^K + (1/3) G_{ijkl}^{IJKL} \psi_j^J \psi_k^K \psi_l^L = P_i^I \quad (29)$$

where the arrays of stiffness coefficients, K , F and G , are expressed in terms of $\sigma_{\lambda,i,q}^I$, the quantities defined by equation (21), and the C 's, F 's and D 's of equation (4). The linear stiffness array K_{ij}^{IJ} is given by

$$K_{ij}^{IJ} = \epsilon_{\lambda,i,q}^I \sigma_{\lambda,j,q}^J \quad (30)$$

wherein λ is summed from 1 to 8 and q is summed from 1 to n_q . The nonlinear stiffness arrays F_{ijk}^{IJK} and G_{ijkl}^{IJKL} have more complex definitions and are specified in the computer program (see also ref. 7).

In equation (29) the arrays K , F and G may be thought of as having only two, three and four indices, respectively, if pairs of indices, each pair consisting of an upper index and the index directly beneath it, are replaced by a single index ranging from 1 to 80. Then, after assembling the contributions from all the elements, the discretized equations have the form

$$K_{\underline{ij}} \psi_{\underline{j}} + (1/2) F_{\underline{ijk}} \psi_{\underline{j}} \psi_{\underline{k}} + (1/3) G_{\underline{ijkl}} \psi_{\underline{j}} \psi_{\underline{k}} \psi_{\underline{l}} = P_{\underline{i}} \quad (31)$$

where the underscored indices range from 1 to 5 N and N is the total number of nodes in the structure. Equation (31) is solved by Newton-Raphson iteration using at the n^{th} step the equations

$$\begin{aligned} & (K_{\underline{ij}} + F_{\underline{ijk}} \psi_{\underline{k}}^{(n)} + G_{\underline{ijkl}} \psi_{\underline{k}}^{(n)} \psi_{\underline{l}}^{(n)}) \Delta \psi_{\underline{j}}^{(n)} \\ & = P_{\underline{i}} - K_{\underline{ij}} \psi_{\underline{j}}^{(n)} - (1/2) F_{\underline{ijk}} \psi_{\underline{j}}^{(n)} \psi_{\underline{k}}^{(n)} - (1/3) G_{\underline{ijkl}} \psi_{\underline{j}}^{(n)} \psi_{\underline{k}}^{(n)} \psi_{\underline{l}}^{(n)} \\ \psi_{\underline{i}}^{(n+1)} & = \psi_{\underline{i}}^{(n)} + \Delta \psi_{\underline{i}}^{(n)} \end{aligned} \quad (32)$$

SYMMETRY CONSIDERATIONS

Special attention is given to the symmetry properties of the arrays of stiffness coefficients. The symmetries are of two very different types — symmetry of the arrays under permutations of the array indices, and symmetry under interchange of the two tangential coordinate directions.

The permutational symmetry is symmetry in the sense that the components in the upper triangular part of a symmetric matrix are copies of the components in the lower triangular part. The element stiffness coefficients arrays in equation (29), K_{ij}^{IJ} , F_{ijk}^{IJK} and G_{ijkl}^{IJKL} , are constructed so as to be totally symmetric under the interchange of any upper-lower pair of indices with any other such pair. This means that nearly half of the components in the array K_{ij}^{IJ} are copies of other components in the array K_{ij}^{IJ} , that approximately one sixth of the components of the array F_{ijk}^{IJK} are independent, and that only approximately one twenty-fourth of the components of the array G_{ijkl}^{IJKL} are independent. For this reason and because of the large number of coefficients, it is important to deal only with the independent components so as not to generate or store an unnecessarily large number of coefficients. For this project the computer implementation of the permutational symmetries is complicated by the fact that the nonlinear arrays are so large that only portions of them can be held in computer memory at any one instant of time.

The second type of symmetry refers not to equal numerical values (as in the first type) but to symmetry in the underlying algebraic expressions. Taking this type of symmetry into account allows one block of computer code to be used for the generation of two different sets of numerical values. This reduces the amount of computer code and simplifies debugging.

Neither of these symmetry considerations is to be confused with the presence or absence of spatial symmetry in the tire configuration.

COMPUTATIONAL PROCEDURE

The first major computational goal is the evaluation of the characteristic arrays K_{ij}^{IJ} , F_{ijk}^{IJK} , G_{ijkl}^{IJKL} and P_i^I for each finite element. For this Gaussian

quadrature is used with index q ranging from 1 to $n_q = 25$. The characteristic arrays are evaluated only once and are saved on disk files for repeated subsequent use.

Preliminaries to the Generation of the Elemental Characteristic Arrays

As a preliminary to the evaluation of the elemental characteristic arrays, the geometric quantities $A_1, A_2, k_1, k_2, a_1, a_2$ (see eqs. (7) and (17)) are evaluated at the quadrature points of an element. Then the shape functions and the strain approximation functions are evaluated at the quadrature points (see eqs. (20) and (21)). In order to exploit the symmetry of the algebraic form of the finite element equations under the interchange of the X_1 and X_2 coordinate directions, a new quadrature index Q ranging from 1 to $2 n_q$ is introduced. The new index Q is equal to either q or $q + n_q$. The arrays of strain approximation function values (with the Q index as the last index in the FORTRAN implementation) are stored such that the index Q for retrieval may range from 1 to n_q or from $n_q + 1$ to $2 n_q$. This is achieved through the use of an ordering such as the following:

$$D_{1,i,q}, D_{2,i,q}, D_{1,i,Q}; a_{1,i,q}, a_{2,i,q}, a_{1,i,Q}; \text{ etc.} \quad (33)$$

such that if the array $D_{1,i,Q}$ is referenced with index Q in the range 1 to n_q , then one retrieves $D_{1,i,q}$ as expected, but if the array $D_{1,i,Q}$ is referenced with index Q in the range $n_q + 1$ to $2 n_q$, what is retrieved is the corresponding value of $D_{2,i,q}$. Similarly, the appropriate value of $D_{1,i,q}$ is retrieved if $D_{2,i,Q}$ is referenced with index Q in the range $n_q + 1$ to $2 n_q$. This scheme is used to reduce the amount of FORTRAN code and the amount of debugging effort.

Since the present implementation is for linearly elastic materials only, the shell stiffnesses (the C 's, F 's and D 's) occur linearly in the stiffness coefficients. Thus it is convenient, in the interests of producing efficient code, to evaluate arrays of coefficients $w_q \bar{C}_{\lambda\mu}$ each of whose entries consist of a shell stiffness $\bar{C}_{\lambda\mu}$ multiplied by a weight w_q . The weight w_q , in turn, is the product of a quadrature weight times two Jacobians. The first Jacobian comes from the transformation from local finite element coordinates to the surface coordinates X_1, X_2 ; and the second one, whose value is $A_1 A_2$, comes from the transformation

from X_1, X_2 to the Cartesian coordinates x_1, x_2, x_3 . For the computation of the F and G arrays these arrays of coefficients are stored redundantly as in equation (33) so that again the index Q may range either from 1 to n_q or from $n_q + 1$ to $2 n_q$. Switching ranges of the index Q results in the transformation

$$\begin{aligned} C_{11} &\leftrightarrow C_{22} \\ C_{16} &\leftrightarrow C_{26} \\ F_{11} &\leftrightarrow F_{22} \\ F_{16} &\leftrightarrow F_{26} \end{aligned} \quad (34)$$

Elements of the array $\sigma_{\lambda,i,q}^I$ are generated in the course of evaluating the K_{ij}^{IJ} and are saved for use in the evaluation of the F_{ijk}^{IJK} .

Generation of the Elemental Characteristic Arrays

The elemental linear stiffness array [K] may be represented in the form

$$K_{ij}^{IJ} \quad (I, J = 1 \rightarrow 5; i, j = 1 \rightarrow 16) \quad (35)$$

where

$$K_{ij}^{IJ} = K_{ji}^{JI}. \quad (36)$$

The components of [K] are generated and stored as 15 blocks of data corresponding to the subarrays

$$\begin{aligned} [K^{11}], [K^{22}], [K^{33}], [K^{44}], [K^{55}], [K^{21}], [K^{31}], [K^{32}], \\ [K^{41}], [K^{42}], [K^{43}], [K^{51}], [K^{52}], [K^{53}], [K^{54}] \end{aligned} \quad (37)$$

The five diagonal blocks represent symmetric arrays and consequently contain $(16 \cdot 17)/2! = 136$ components each. The ten off-diagonal blocks are stored in full and contain $16^2 = 256$ components each. A partition such as $[K^{12}]$ is merely the transpose of $[K^{21}]$ and thus is neither separately evaluated nor stored. There is no problem keeping the 3240 independent components of [K] in memory at one time.

The elemental stiffness array [F] may be represented in the form

$$F_{ijk}^{IJK} \quad (I, J, K = 1 \rightarrow 5; i, j, k = 1 \rightarrow 16) \quad (38)$$

where

$$F_{ijk}^{IJK} = F_{jki}^{JKI} = F_{kij}^{KIJ} = F_{jik}^{JIK} = F_{kji}^{KJI} = F_{ikj}^{IKJ} \quad (39)$$

Because the nonlinear parts of the strains are independent of ϕ_1 and ϕ_2 (see eqs. (5) and (6)), it follows that any component of F_{ijk}^{IJK} with any two of the I, J or K equal to 4 or 5 must be zero. Consequently, the independent blocks of [F] are

$$\begin{aligned} & [F^{111}], [F^{222}], [F^{333}], \\ & [F^{211}], [F^{122}], [F^{311}], [F^{133}], [F^{322}], [F^{233}], \\ & [F^{411}], [F^{422}], [F^{511}], [F^{522}], [F^{433}], [F^{533}], \\ & [F^{321}], [F^{421}], [F^{521}], [F^{431}], [F^{531}], [F^{432}], [F^{532}] \end{aligned} \quad (40)$$

The three diagonal blocks $[F^{111}]$, $[F^{222}]$ and $[F^{333}]$ each have $16 \cdot 17 \cdot 18 / 3! = 816$ independent components, and the three are kept together in memory. The 12 semidiagonal blocks each have $16 \cdot (16 \cdot 17 / 2!) = 2176$ independent components, and only two such blocks are kept in memory simultaneously. Finally, the seven offdiagonal blocks each have $16^3 = 4096$ components, and only one is kept in memory at a time. Thus the 57232 independent components of the elemental F array are stored on disk in 14 separate records, and no more than 4352 entries are in memory at any one time.

The elemental stiffness array [G] may be represented in the form

$$G_{ijkl}^{IJKL} \quad (I, J, K, L = 1 \rightarrow 5; i, j, k, l = 1 \rightarrow 16) \quad (41)$$

where

$$G_{ijkl}^{IJKL} = G_{jikl}^{JIKL} = \text{etc.} \quad (42)$$

Because of equations (5) and (6), the range of the upper indices is limited to $1 \rightarrow 3$ rather than from $1 \rightarrow 5$. The independent subarrays of [G] are

$$\begin{aligned}
& [G^{1111}], [G^{2222}], [G^{3333}], \\
& [G^{2111}], [G^{1222}], [G^{3111}], [G^{1333}], [G^{3222}], [G^{2333}], \\
& [G^{2211}], [G^{3311}], [G^{3322}], \\
& [G^{3211}], [G^{3122}], [G^{2133}]
\end{aligned} \tag{43}$$

The diagonal subarrays of the form $[G^{IIII}]$ have $16 \cdot 17 \cdot 18 \cdot 19 / 4! = 3876$ independent components each; the subarrays of the form $[G^{IJJJ}]$ ($I \neq J$) each have $16 \cdot (16 \cdot 17 \cdot 18 / 3!) = 13056$ components; the subarrays of the form $[G^{IIJJ}]$ ($I > J$) each have $(16 \cdot 17 / 2!)^2 = 18496$; and finally, the subarrays $[G^{IJKK}]$ ($I > J \neq K \neq I$) each have $16^2 \cdot (16 \cdot 17 / 2!) = 34816$ components. Apart from the three diagonal subarrays, the sizes of the G subarrays are too large to keep whole subarrays in memory at any one time. The program stores the 249,900 components of the elemental G array in 66 records and holds no more than 4352 in memory at any one time. If the full G array were to be stored, it would occupy more than 21 times as much memory as is used by the scheme implemented.

The strain approximation functions (eq. (20)) and the elemental stiffness arrays (eq. (29)) are never evaluated more than once for a given element during the course of a computer run. This approach results in the storage on disk of more than 300,000 coefficients for each "distinct" finite element. While this number is large, the same coefficients are used many times in the course of developing the response of the tire to varying loads. Fortunately, in laying out the nodal points of the tire shell, the same geometry may be used for several elements. Thus the number of distinct elements may be considerably fewer than the total number of finite elements.

Use of the Elemental Characteristic Arrays

The elemental characteristic arrays are used for generating the coefficients of the Newton-Raphson equations (32), for generating the basis vectors and the coefficients of the reduced system of equations [see refs. 3 through 6], and in the postprocessing phase for evaluating the various contributions to the total strain energy. These applications require evaluation of the products of K_{ij}^{IJ} , F_{ijk}^{IJK} and G_{ijkl}^{IJKL} with the solution vector X_i^I and its derivatives \dot{X}_i^I , \ddot{X}_i^I , \dddot{X}_i^I , etc. with respect

to some specified parameter which varies along the solution path. The subroutines which evaluate these products are considerably complicated by the fact that only the independent components of the characteristic arrays are stored. This is especially true for the subroutine which generates the array

$$GX_{ijk}^{IJK} = G_{ijkl}^{IJKL} X_l^L \quad (44)$$

because neither the whole of G nor the whole of GX can be kept in memory. However, this complication is more than offset by the storage reduction it allows.

SAMPLE PROBLEMS

Two sample problems are considered in this report. The first is a thin-walled isotropic torus under uniform interior or exterior pressure (previously analyzed with a fixed external pressure in ref. 8). The second is a laminated toroid with elliptical cross section having two clamped edges corresponding to the beads of a tire. The toroid is pressurized from within. Both problems have axially symmetric loads even though the computer code is designed for general load distributions.

Symmetries

The presence of symmetric configurations in the sample problems allows a very sizeable reduction in the number of degrees of freedom needed to achieve the desired levels of accuracy. Because of the axial symmetry of both the undeformed shell and the loads, the solutions are expected to be axially symmetric at least for the cases of internal pressure or moderate external pressure. Consequently, a single strip of finite elements is employed to cover the range of azimuthal angles and the circumferential angle in each element ranges from 0 to 2π . The total number of degrees of freedom is further reduced by letting all nodes with the same azimuthal angle be constrained to have the same displacements.

In addition to axial symmetry, both problems exhibit symmetry under rotations by 180° about a set of axes normal to the main axis (i.e., the axis of axial symmetry). As a consequence, the generalized displacement functions u_1 , u_2 , ϕ_1 and ϕ_2 all change sign under reflection in a plane normal to the main axis, while the normal displacement w is left invariant under such a reflection. It follows that

by imposing the appropriate boundary conditions it is necessary to model only one side of the shells. It may also be noted that for isotropic materials the functions u_2 and ϕ_2 must be invariant under the reflection referred to above. Consequently, it follows that $u_2 = 0$ and $\phi = 0$, and the number of degrees of freedom is even further reduced.

First Sample Problem

The geometry of the torus in the first sample problem is shown in Fig. 2. The torus has cross-sectional radius a , toroidal radius b , thickness h and material properties typical of an aluminum alloy. There are no boundary constraints other than those which rule out the rigid body motions. The deformation for a uniform external pressure $p = -0.6895 \cdot 10^6 \text{ N/m}^2$ (100 psi) is shown in Fig. 3. In that figure the middle surface of the undeformed shell is represented by the circle and the short lines indicate the displacements of representative material points on the reference surface. The displacements have been multiplied by a factor of hundred. Because of the material isotropy, u_2 and ϕ_2 are zero and the displacements are all in the plane of the cross section. The variation of the normal displacement w with X_1 is shown in Fig. 4 for the same external pressure. The results are in close agreement with the results reported in ref. 8. The inner diameter remains nearly unchanged. The normal displacement of a series of points in the middle surface of the shell is shown as a function of pressure in Fig. 5. The shell appears to collapse at an external pressure of approximately $1.04 \cdot 10^6 \text{ N/m}^2$ (150 psi). Because for large external pressures there are several distinct maxima and minima in the displacement components as functions of azimuthal angle, it is necessary to use several finite elements to get good accuracy. Twelve elements were used for the data presented in Fig. 3, and sixteen in Fig. 4. For an external pressure of $0.6985 \cdot 10^6 \text{ N/m}^2$ (100 psi) values of the normal displacement at $X_1 = 0$ (near the point of maximum displacement) and at $X_1 = \pi/2$ (the outside diameter) are shown in Table 1 as a function of the number of elements in the half toroid. Far fewer elements are needed to get comparable accuracy for the case of internal pressure.

Second Sample Problem

The geometry of the toroid in the second sample problem is shown in Fig. 6. The toroid has an elliptical cross section with semimajor axis a and eccentricity

e. The toroidal radius is b and the thickness is h . The shell is clamped along two parallel circles a distance c apart. The shell consists of ten layers of fibrous material with orientation angles alternately 45° and -45° with respect to the circumferential direction. The material properties are chosen to correspond roughly to those of the cords of an aircraft tire. The displacements in the plane of the cross section caused by a uniform internal pressure $p = 2.413 \cdot 10^6 \text{ N/m}^2$ (350 psi) is shown in Fig. 7. The middle surface of the unpressurized shell is represented by the inner (elliptical) curve, and the middle surface of the pressurized shell is represented by the outer curve. The short lines connect material points in the unpressurized and pressurized configurations. The displacements are not magnified. The displacements in the circumferential direction are nonzero but not shown here.

CONCLUDING REMARKS

A computer program has been constructed for static analysis of geometrically-nonlinear deep laminated shells of revolution. The program performs well for the sample problems to which it has been applied and appears to provide a good foundation for future tire analysis work. Future research in this area should address such subjects as configuration dependent loading, tire contact loads, large shell rotations, more general shell geometries to simulate actual tire cross sections, and more realistic tire material properties including the nonhomogeneous aspects of tire construction.

REFERENCES

1. Sanders, J. Lyell., Jr: "Nonlinear Theories for Thin Shells", Quarterly of Applied Mathematics, vol. 21, no. 1, April 1963, pp. 21-36.
2. Budiansky, B.: "Notes on Nonlinear Shell Theory", Journal of Applied Mechanics, vol. 35, series E, no. 2, June 1968, pp. 393-401.
3. Noor, A. K. and Peters, J. M.: "Reduced basis technique for nonlinear analysis of structures", AIAA J., Vol. 18(4), 1980, pp. 455-462.

4. Noor, A. K.; Andersen, C. M. and Peters, J. M.: "Global-local approach for nonlinear shell analysis", Proceedings of the Seventh ASCE Conference on Electronic Computation, August 6-8, 1979, Washington University, St. Louis, Missouri, pp. 634-657.
5. Noor, A. K. and Peters, J. M.: "Nonlinear analysis via global-local mixed finite element approach", International Journal for Numerical Methods in Engineering, vol. 15, no. 9, 1980, pp. 1363-1380.
6. Noor, A. K.: "Recent advances in reduction methods for nonlinear problems", Computers and Structures, Vol. 13, 1981, pp. 31-44.
7. Noor, A. K. and Andersen, C. M.: "Computerized symbolic manipulation in nonlinear finite element analysis", Computers and Structures, Vol. 13, 1981, pp. 379-403.
8. Chan, A. S. L. and Trbojevic, V. M.: "Thin Shell Finite Element by the Mixed Method Formulation - Parts 2 and 3", Computer Methods In Applied Mechanics and Engineering, Vol. 10, 1977, pp. 75-103.

Table 1. Values of normal displacement w for the shell of Fig. 2 for varying number of finite elements modeling the half torus. Displacements are shown for $X_1 = 0$ and $\pi/2$ radians. Pressure = $-0.6895 \cdot 10^6 \text{ N/m}^2$ (100 psi).

number of elements	number of d. o. f.	w_0	$w_{\pi/2}$
4	65	-0.021483	-0.0065057
8	125	-0.026082	-0.0065973
12	185	-0.029227	-0.0066134
16	245	-0.029784	-0.0066225

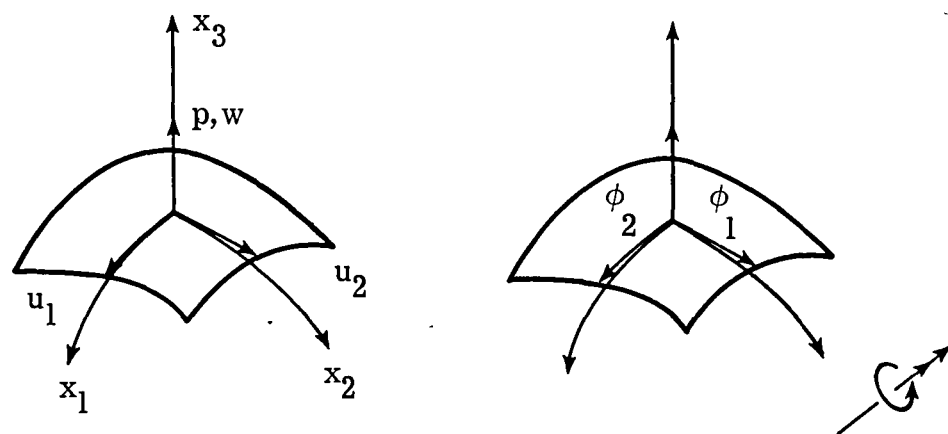


Figure 1. Shell element and sign convention.

$$E = 68.95 \cdot 10^9 \text{ N/m}^2 \quad (10^7 \text{ psi})$$

$$\nu = 0.3$$

$$a = 25.4 \text{ cm} \quad (10 \text{ in.})$$

$$b = 38.1 \text{ cm} \quad (15 \text{ in.})$$

$$h = 0.254 \text{ cm} \quad (0.1 \text{ in.})$$

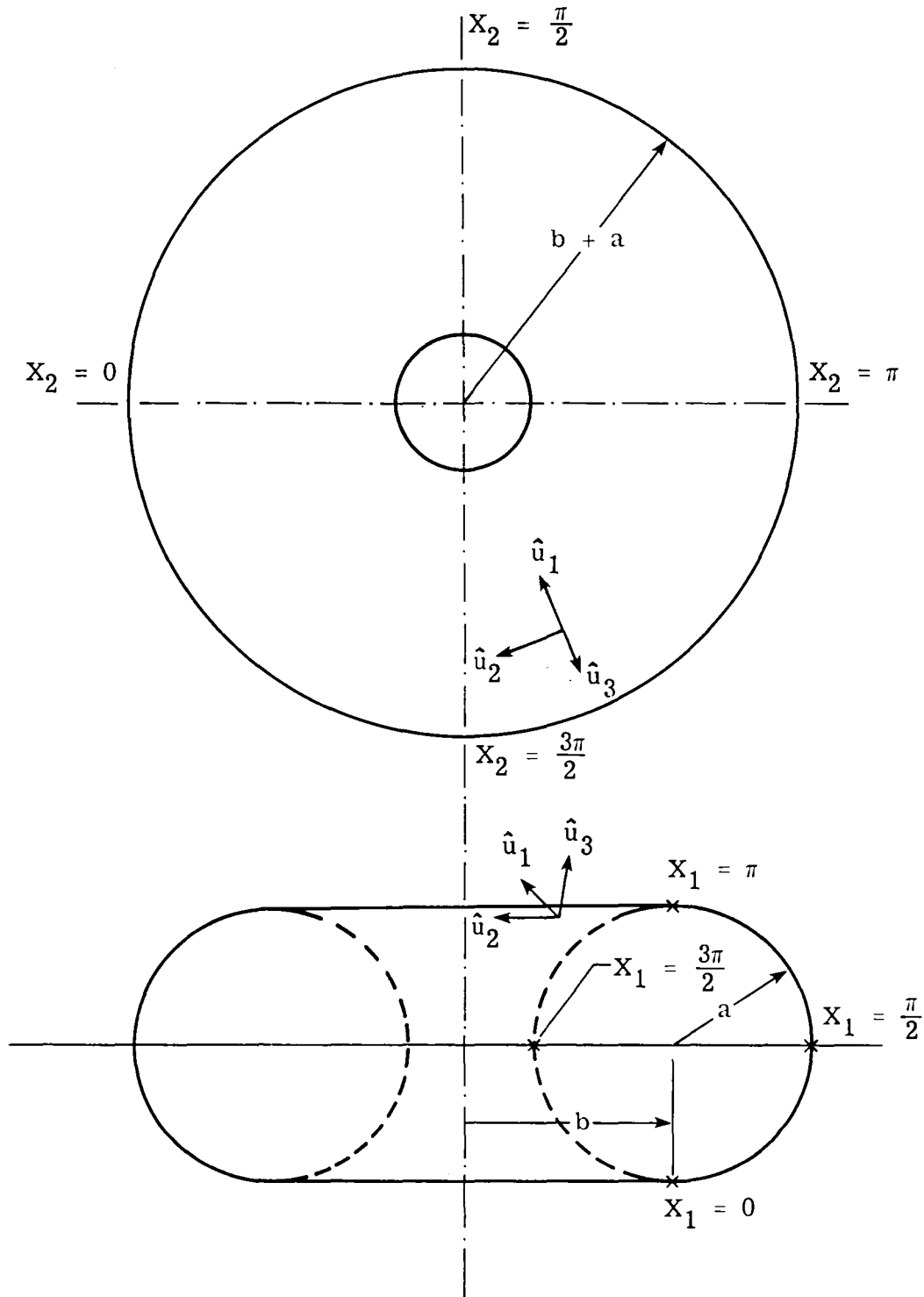


Figure 2. Geometry of toroidal shell with circular cross section.

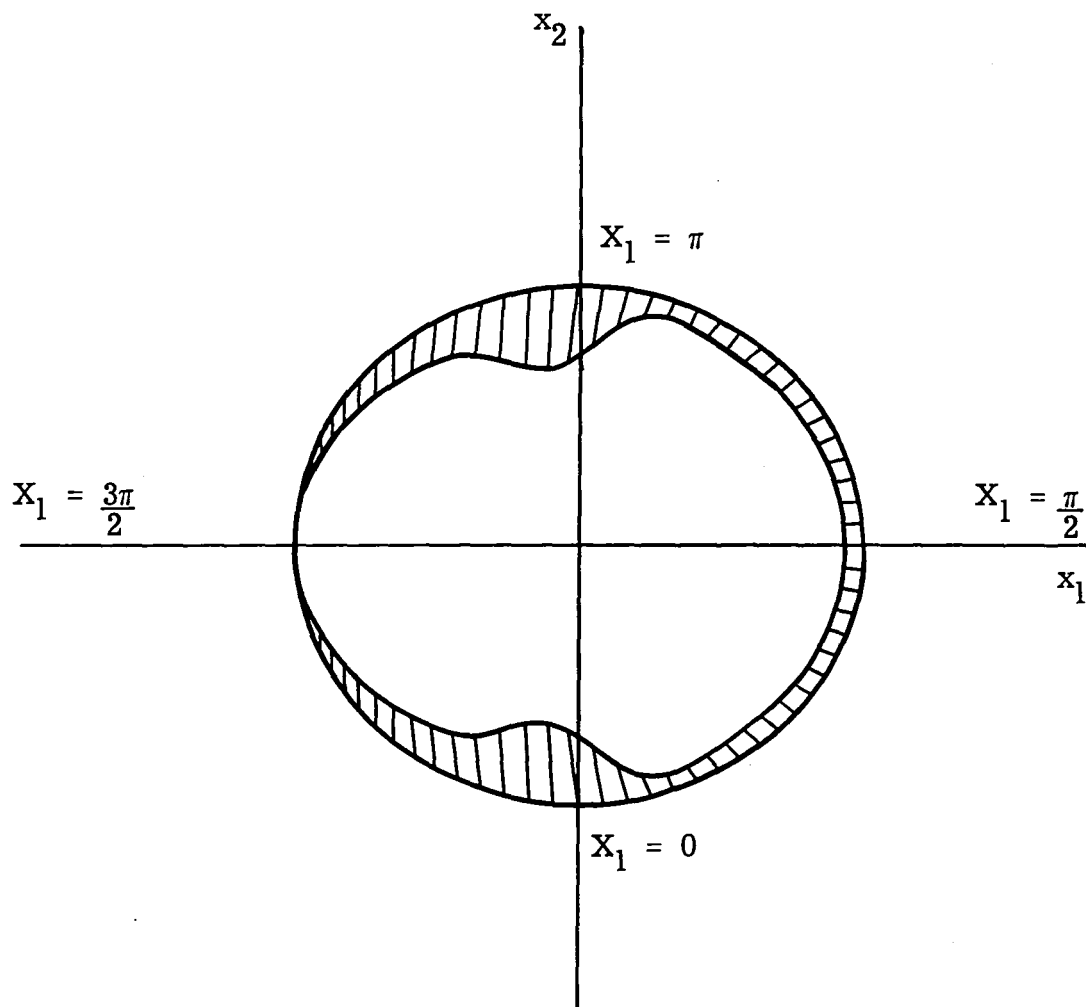


Figure 3. Deformation of middle surface torus of Fig. 2 due to uniform external pressure $p = -0.6895 \cdot 10^6 \text{ N/m}^2$ (100 psi). Displacements shown are 100 times the actual displacements. Twelve finite elements.

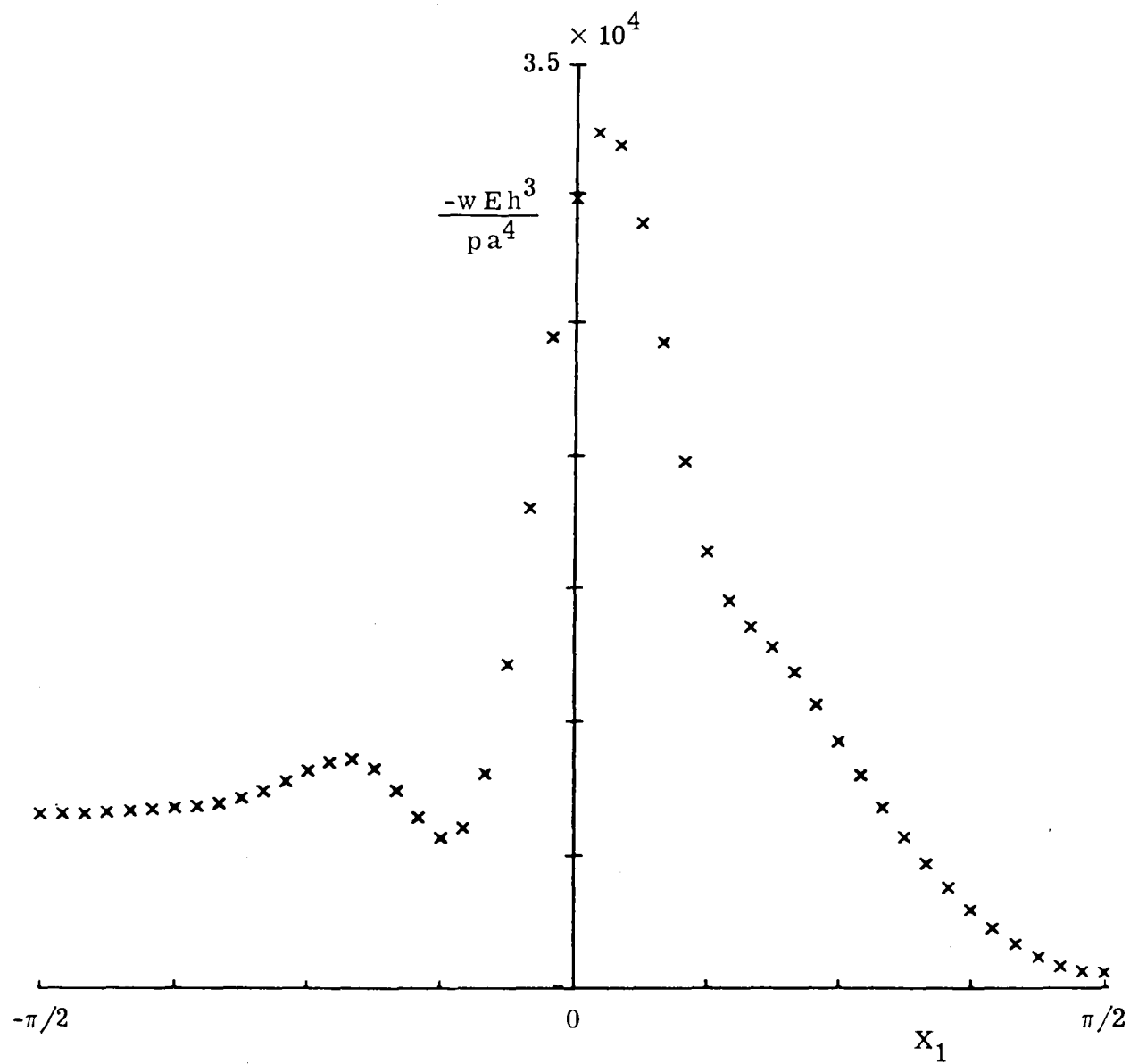


Figure 4. Normal displacement w vs. angle X_1 for uniform external pressure $p = -0.6895 \times 10^6 \text{ N/m}^2$ (100 psi). Sixteen finite elements.

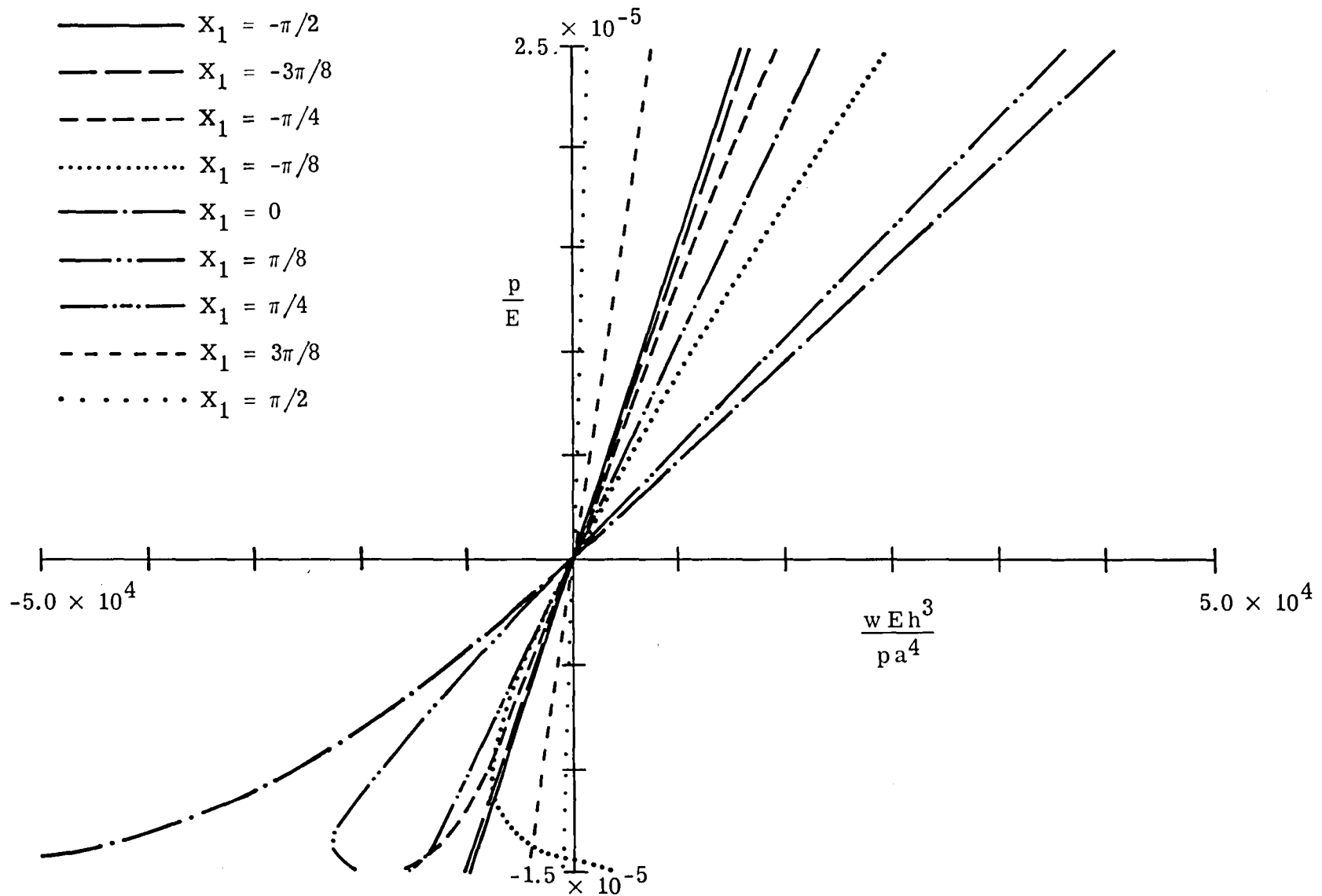


Figure 5. Normal displacements for representative points on the middle surface of the torus (see Fig. 2) shown as a function of pressure p . Positive (negative) p corresponds to internal (external) pressure.

$$a = 6.223 \text{ cm} \quad (2.45 \text{ in.})$$

$$b = 18.87 \text{ cm} \quad (7.7 \text{ in.})$$

$$c = 10.16 \text{ cm} \quad (4.0 \text{ in.})$$

h = 1.029 cm (0.42 in.)

$$e = 0.5$$

$$\nu_{LT} = 0.4$$

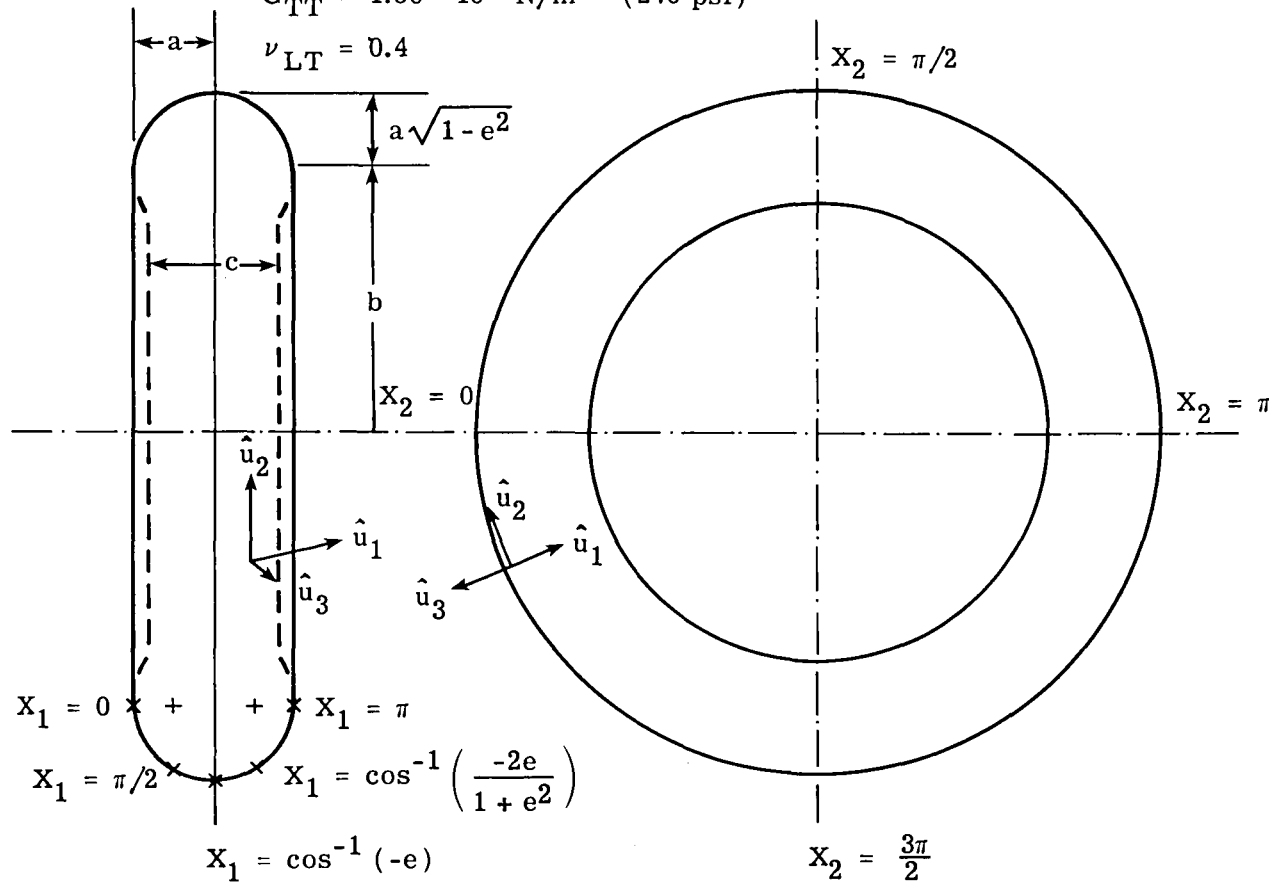


Figure 6. Geometry of toroidal model of a tire. The cross section of an ellipse with foci indicated by the plus signs. Clamped boundary conditions are assumed along the two innermost diameters, $X_1 = X_1^0$. The ten equal-thickness layers have fiber angles which are alternately 45° and -45° with respect to the circumferential direction.

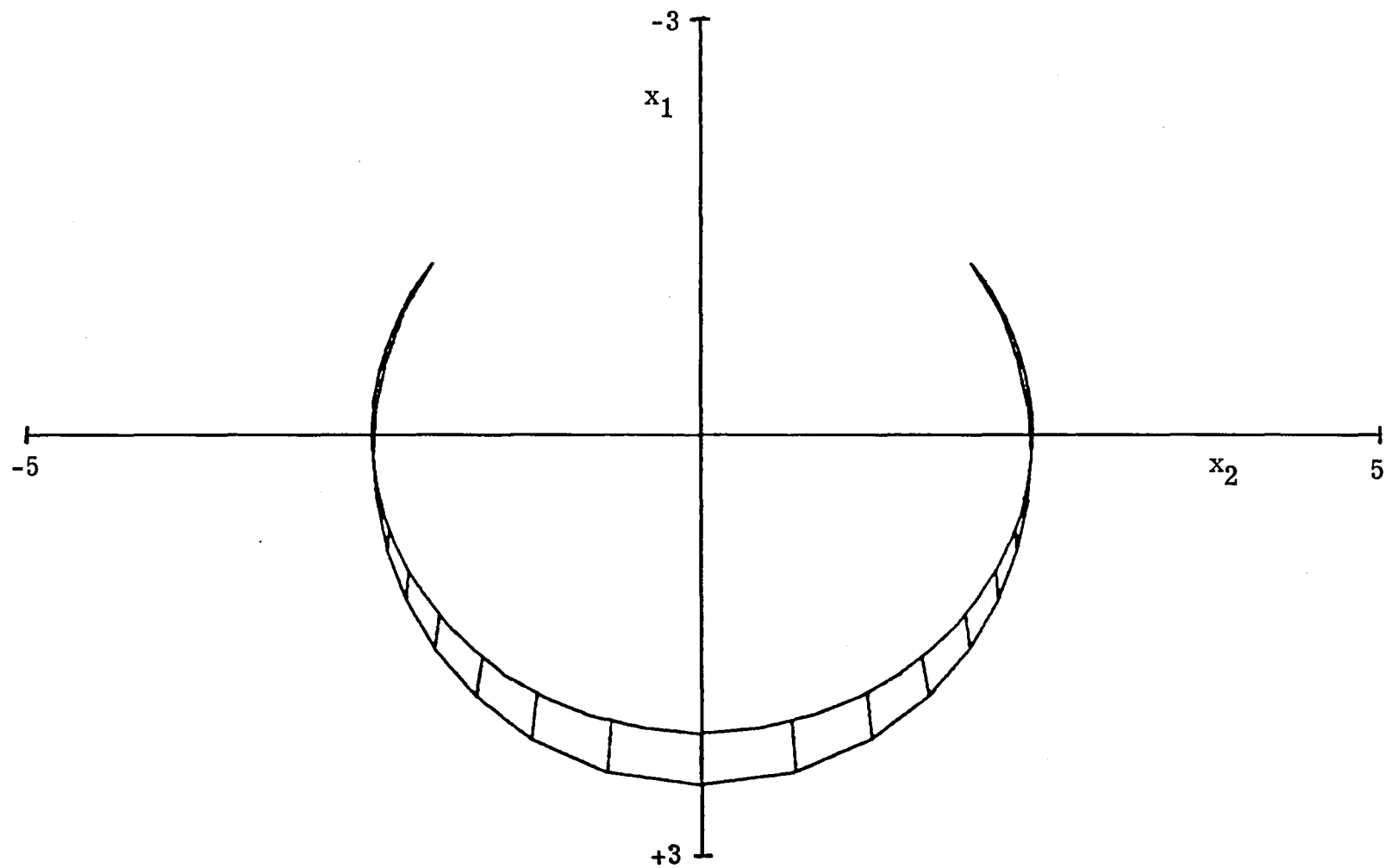


Figure 7. Deformation (in the plane of the cross section) of the toroidal shell shown in Fig. 5 due to uniform internal pressure $p = 2.413 \cdot 10^6 \text{ N/m}^2$ (350 psi). Displacements are shown true to scale.

End of Document